Radial and angular correlations and the classification of intershell $2l2l'3l''$ triply excited states of atoms

Toru Morishita[1] and C. D. Lin[2]
[1]*Department of Applied Physics and Chemistry, University of Electro-Communications, 1-5-1 Chofu-ga-oka, Chofu-shi, Tokyo 182-8585, Japan*
[2]*Department of Physics, Kansas State University, Manhattan, Kansas 66506*
(Received 9 September 2002; published 28 February 2003)

We analyzed radial and angular correlations of 50 $2l2l'3l''$ triply excited states of atoms. Using hyperspherical coordinates, we examined channel wave functions in the body-fixed frame to identify elementary normal modes of the correlated motion of the three electrons. For these states, we showed that the bending vibrational modes characterizing the angular correlations are the same as those in $2l2l'2l''$ and $3l3l'3l''$ intrashell states, but additional "+" or "−" quantum numbers are needed to distinguish the symmetric or antisymmetric stretch of the outer electron with respect to the two inner ones for the $2l2l'3l''$ intershell states.

DOI: 10.1103/PhysRevA.67.022511 PACS number(s): 31.15.Ja, 31.10.+z, 31.25.Jf, 31.30.−i

I. INTRODUCTION

Since the advent of quantum mechanics, the description of a many-electron atom is based mostly on the independent particle model (IPM). In this model, each electron is described to be under the influence of a mean field due to the other electrons and the field from the nucleus. The many-electron atomic states are then designated by a collection of quantum numbers from individual electrons. Such an IPM fails completely for doubly excited states of atoms where two electrons are simultaneously excited. Doubly excited states of an atom can be separated into two types. The first type is intrashell doubly excited states where the two electrons are at about equal distances from the nucleus. These states have been classified in terms of the K and T quantum numbers, as introduced initially by Herrick and Sinanoğlu [1,2] based on the SO(4) group. Subsequently, it was understood that K describes the bending vibration of the two electrons and T is a projection of the orbital angular momentum with respect to the quantization axis of the body-fixed frame which is taken to be along the interelectronic line. These later works pointed out the importance of examining electron correlations in the body-fixed frame of atoms and to borrow ideas from molecular physics [3–7]. Thus, intrashell doubly excited states can then be visualized as analogous to the rovibrational motion of a linear XY_2 molecule, with X being the nucleus and Y the electron. The second type of states are intershell doubly excited states, where the distances of the two electrons from the nucleus are quite different. To describe the joint radial motion of the two electrons, an important concept, the so-called "+" and "−" quantum numbers, was first introduced by Cooper, Fano, and Prats [8]. From the mechanistic viewpoint, in the + states, the two electrons move toward or away from the nucleus together in phase. For the−states, the radial motions of the two electrons are out of phase—thus when one electron moves toward the nucleus, the other moves away from it, and vice versa. The failure of the IPM for doubly excited states of atoms are now well understood. Various new approaches have been developed for understanding the joint motion of the pair of electrons, including semiclassical methods. In spite of differences in the language and methods used in these treatments, the conclusions are identical, i.e., the correlated motion of the two electrons in doubly excited states of an atom can be classified in terms of molecular modes. Accurate numerical calculations and experimental data have been obtained for the doubly excited states in He in the past two decades and this mature field has been nicely reviewed recently by Tanner *et al.* [9]. We also comment that such molecular modes have also been identified in two-electron quantum dots in a confined magnetic field [10].

Since intrashell and intershell states of an atom can also be grouped together to form a Rydberg series, the K and T quantum numbers and the + and − quantum numbers can be combined, such that each doubly excited state is designated by ${}_n(K,T)^A_N$ [6], where n and N are the approximate principal quantum numbers of each electron and $A=+$ or − is the symmetry in the radial motion. When radial correlation is not significant, $A=0$ was also introduced to describe such states. For intrashell states, $n=N$, and $A=+$ only. Thus, ${}_n(K,T)^A_N$ are the new approximate quantum numbers that replace the $nlNl'$ quantum numbers from the IPM, and doubly excited states are understood in terms of the bending vibrational motion and the stretch of the two electrons. For low-lying doubly excited states, the ${}_n(K,T)^A_N$ classification is adequate and such designations are now widely used in describing doubly excited states. We comment that this classification is not expected to be valid for very high-lying doubly excited states, where the concept of principal quantum numbers does not exist any more.

After the successful classification of doubly excited states, clearly the next objective is to look for the classification of triply excited states. Unlike doubly excited states of an atom, few approaches have been available for the classification of these states. An early attempt along this direction for intrashell triply excited states had been made by Watanabe and Lin [11] where they examined a model atom of three electrons on the surface of a sphere, similar to the work of Ezra and Berry [5] for their model study of two-electron atoms. Subsequent investigations by Bao *et al.* [12] showed that

TABLE I. Present classifications and independent particle model (IPM) classifications of the $2l2l'3l'$ intershell triply excited states of Li. Energy levels and IPM classifications are taken from Conneely and Lipsky [27]. In IPM classifications, *A*, *B*, *C*, *D*, *E*, and *F* stand for the Li^+ core states of $2s^2\,^1S^e$, $2s2p\,^3P^o$, $2p^2\,^3P^e$, $2p^2\,^1D^e$, $2s2p\,^1P^o$, and $2p^2\,^1S^e$, respectively. The energy levels of those core states are $-1.897\,023\,0$, $-1.870\,280$, $-1.785\,150$, $-1.752\,300$, $-1.738\,230$, and $-1.602\,650$ a.u., respectively. N_T are the fractions of the rotational decomposition of the hyperspherical channel functions at the hyper-radius R_0 where the hyper-radial wave function is near the maximum for that state.

States	Group T	IPM	Energy (a.u.)	N_T $T=0$	$T=1$	$T=2$	$T=3$	$T=4$	R_0 (a.u.)
$^2S^e$									
(1)	A^{+-}-0	*A* 3*s*	−2.004837	1.00					6.3
(2)	C^{++}-0	*B* 3*p*	−1.941499	1.00					6.3
(3)	C^{+-}_{sh}-0	*E* 3*p*	−1.846667	1.00					4.5
(4)	C^{+-}_{ss}-0	*D* 3*d*	−1.806143	1.00					6.2
(5)	C^{+-}_{hh}-0	*F* 3*s*	−1.655855	1.00					6.0
$^2S^o$									
(1)	B^{+-}-0	*C* 3*p*	−1.883344	1.00					6.0
$^2P^e$									
(1)	A^{+-}-0	*B* 3*p*	−1.971677	0.86	0.14				4.7
(2)	B^{++}-1	*C* 3*s*	−1.878293	0.40	0.60				4.7
(3)	C^{+-}_{h}-0	*C* 3*d*	−1.849150	0.38	0.62				6.1
(4)	B^{+-}-1	*E* 3*p*	−1.841264	0.42	0.58				6.1
(5)	C^{+-}_{s}-0	*D* 3*d*	−1.807407	0.71	0.29				6.1
$^2P^o$									
(1)	A^{+-}-1	*A* 3*p*	−1.987946	0.05	0.95				6.0
(2)	A^{++}-1	*B* 3*s*	−1.965687	0.04	0.96				6.1
(3)	C^{+-}_{s}-1	*B* 3*d*	−1.927816	0.21	0.79				6.0
(4)	B^{+-}-0	*E* 3*s*	−1.866322	0.27	0.73				6.0
(5)	C^{++}-1	*C* 3*p*	−1.856718	0.07	0.93				6.0
(6)	C^{+-}_{h}-1	*D* 3*p*	−1.820848	0.17	0.83				5.8
(7)	C^{+-}_{sh}-1	*E* 3*d*	−1.807621	0.25	0.75				5.8
(8)	C^{+-}_{hh}-1	*F* 3*p*	−1.692512	0.10	0.90				5.8
$^2D^e$									
(1)	A^{+-}-2	*A* 3*d*	−1.961412	0.17	0.04	0.79			6.1
(2)	A^{++}-2	*B* 3*p*	−1.952783	0.07	0.08	0.85			6.2
(3)	C^{+-}_{h}-2	*C* 3*d*	−1.843620	0.06	0.22	0.72			6.1
(4)	C^{+-}_{s}-2	*E* 3*p*	−1.834940	0.20	0.22	0.58			6.1
(5)	B^{+-}-1	*D* 3*d*	−1.812242	0.32	0.23	0.45			6.1
(6)	A^{+-}-0	*D* 3*s*	−1.806939	0.32	0.27	0.41			6.1
(7)	C^{+-}_{hh}-2	*F* 3*d*	−1.656244	0.14	0.09	0.77			7.4
$^2D^o$									
(1)	A^{+-}-1	*B* 3*d*	−1.934641	0.11	0.64	0.25			5.8
(2)	A^{++}-1	*C* 3*p*	−1.869067	0.06	0.75	0.19			5.0
(3)	B^{+-}-2	*D* 3*p*	−1.844685	0.12	0.55	0.33			5.8
(4)	C^{+-}_{s}-1	*E* 3*d*	−1.809504	0.06	0.41	0.53			5.8
$^2F^e$									
(1)	A^{+-}-2	*C* 3*d*	−1.847904	0.12	0.08	0.64	0.16		4.0
(2)	B^{+-}-3	*D* 3*d*	−1.824001	0.17	0.20	0.44	0.19		3.9

TABLE I. (*Continued*).

				N_T					
States	Group T	IPM	Energy (a.u.)	$T=0$	$T=1$	$T=2$	$T=3$	$T=4$	R_0 (a.u.)
$^2F^o$									
(1)	A^{+-}-3	$B\ 3d$	−1.930872	0.04	0.20	0.11	0.65		5.0
(2)	C_s^{+-}-3	$D\ 3p$	−1.850577	0.06	0.19	0.12	0.63		8.0
(3)	C_h^{+-}-3	$E\ 3d$	−1.802827	0.08	0.27	0.22	0.43		8.0
$^2G^e$									
(1)	A^{+-}-4	−	−	0.04	0.07	0.13	0.07	0.69	5.5
$^4S^e$									
(1)	C_s^{+-}-0	$B\ 3p$	−1.957118	1.00					5.5
$^4S^o$									
(1)	B^{++}-0	$C\ 3p$	−1.866429	1.00					6.0
$^4P^e$									
(1)	A^{++}-0	$B\ 3p$	−1.957029	0.90	0.10				6.0
(2)	B^{+-}-1	$C\ 3s$	−1.888905	0.40	0.60				6.1
(3)	C_h^{+-}-0	$C\ 3d$	−1.847516	0.40	0.60				6.1
$^4P^o$									
(1)	A^{+-}-1	$B\ 3s$	−1.984064	0.07	0.93				6.0
(2)	C_s^{+-}-1	$B\ 3d$	−1.931807	0.02	0.98				6.0
(3)	C_h^{+-}-1	$C\ 3p$	−1.869121	0.23	0.77				6.0
$^4D^e$									
(1)	A^{+-}-2	$B\ 3p$	−1.965886	0.08	0.11	0.81			5.8
(2)	C_h^{+-}-2	$C\ 3d$	−1.846687	0.05	0.13	0.82			5.2
$^4D^o$									
(1)	A^{+-}-1	$B\ 3d$	−1.938396	0.05	0.85	0.10			6.0
(2)	B^{+-}-2	$C\ 3p$	−1.872317	0.17	0.39	0.44			6.0
$^4F^e$									
(1)	A^{+-}-2	$C\ 3d$	−1.849785	0.33	0.07	0.31	0.29		4.5
$^4F^o$									
(1)	A^{+-}-3	$B\ 3d$	−1.936047	0.01	0.10	0.04	0.85		5.0

quantum symmetry imposes severe constraints on the body-fixed frame wave functions. Namely, the fact that each eigenstate of the model atom has well-defined total angular momentum L, total spin S, and parity π, requires that the wave function in the body-fixed frame to have nodal surfaces due to the symmetry imposed on the wave function. Partial plots of wave functions from this model atom were analyzed and several elementary normal modes were identified. Subsequent studies of triply excited states of atoms follow two general directions. One is the calculation of energy levels and decay widths of individual triply excited states using the standard methods such as the R-matrix method [13–16], the multiconfiguration Hartree-Fock method [17,18], complex-rotation method [19–22], K matrix method [23,24], and configuration interaction (CI) method [25–27]. Experimentally, triply excited states of Li atoms have been investigated using synchrotron radiation [28–34] and partial decay widths of $^2P^o$ and $^2D^e$ states have been measured and the results are compared well with these theoretical calculations [35,36]. However, only a very limited number of triply excited states have been measured or calculated so far.

Another line of theoretical inquiry of triply excited states is the one we have followed. Our main objective is to search for new classifications of triply excited states by exploring the correlated motion of the three electrons and to identify approximate normal modes of their internal degrees of free-

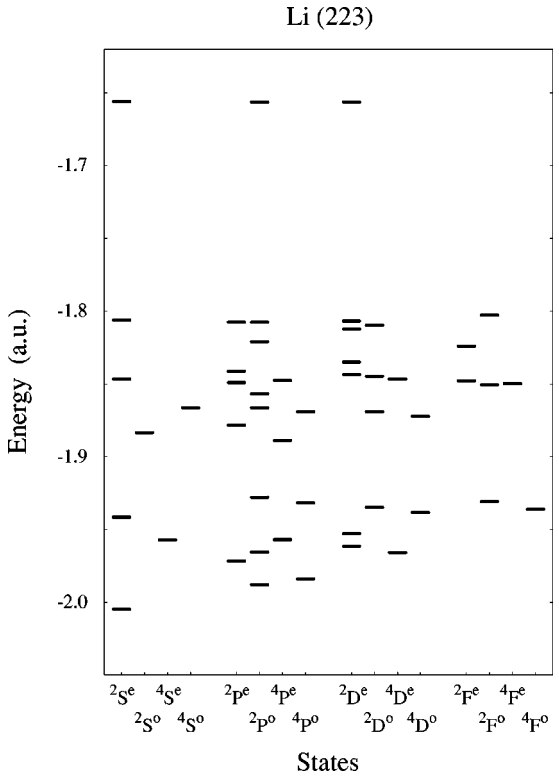

FIG. 1. Energy levels of the $2l2l'3l''$ intershell triply excited states of Li for $L \leqslant 3$. The energies are measured from the triple-ionization threshold. The order along each column is according to the $^{2S+1}L^{\pi}$ symmetry. The relative orders of the spectra exhibit no regularity. Numerical values of the energy levels are taken from Conneely and Lipsky [27].

dom. For this purpose, we need to have an efficient method of calculating the wave functions of triply excited states as well as a means to analyze them. The model atom of three electrons on the surface of a sphere in Ref. [11] serves as a good starting point for the study of intrashell triply excited states without the need to deal with singly and doubly excited states of a real atom.

For the model atom, since each electron is confined to the surface, the three-electron system is governed by six angles. The six-dimensional spatial wave function can be further reduced to three dimensions if the overall rotation of the model atom with respect to the space-fixed axis is removed. To describe the joint motion of the three electrons, the remaining three degrees of freedom should be chosen ''democratically.'' A set of such internal angles were adopted by Bao *et al.* [12], where they further analyzed intrinsic quantum symmetry and the nodal structure of the wave functions in the body-fixed frame. The existence of nodal surfaces in a multidimensional space implies higher energies [37,38]. Thus, by examining the nodal surfaces of the calculated wave functions, the classification of intrashell states becomes possible. For this purpose, probability densities in the three-dimensional space are visualized using contour surfaces [39]. From such an analysis, the eight $2l2l'2l''$ triply excited states were classified into three sets [39,40]. Each set of states can be classified in terms of D_{3h} groups—A_1', A_2'', and the doubly degenerate E' [11]. The three sets are subsequently denoted by *A*, *B*, and *C*, respectively, for simplicity [39,40]. For the 64 $3l3l'3l''$ triply excited states, the excited normal modes of these three elementary groups have also been identified [37,41]. Similar effort of classifying intrashell triply excited states has been undertaken by Madsen and Mølmer [42,43]. For the group of states where the three electrons form a coplanar equilateral triangle with the nucleus at the center (group *A*), they have been able to construct approximate wave functions from a direct product of single-electron Stark states. However, their method has been limited to this elementary group only, where the internal wave function has no nodal surfaces . Their method has not been developed for the classification of all intrashell triply excited states.

In this paper, we set to classify intershell triply excited states. We obtained the wave functions of intershell as well as intrashell states simultaneously using hyperspherical coordinates within the adiabatic approximation. By analyzing the hyperspherical channel wave functions in the body-fixed frame (Sec. II), we showed that quantum symmetries such as *L*, *S*, and π would impose constraints on the body-fixed frame channel functions. From the nature of these constraints, we classify the intershell triply excited states and the results are shown in Sec. III. Section IV summarizes the result and the classification for all the 50 $2l2l'3l''$ intershell states is given in Table I.

II. CALCULATION AND ANALYSIS OF WAVE FUNCTIONS OF TRIPLY EXCITED STATES OF ATOMS

A. Solutions in hyperspherical coordinates

We consider the three-electron atom within the nonrelativistic approximation such that the Schrödinger equation for a three-electron atom is

$$\left[\sum_{i=1}^{3}\left(-\frac{1}{2}\Delta_{\mathbf{r}_i}-\frac{Z}{r_i}\right)+\sum_{i<j}\frac{1}{|\mathbf{r}_i-\mathbf{r}_j|}-E\right]\Psi=0, \qquad (1)$$

where $\mathbf{r}_i$ is the position vector of the ith electron from the nucleus with electric charge *Z*, and *E* is the total energy measured from the triple-ionization threshold. The solution of this equation gives the complete spectra of a three-electron atom, with triply excited states lying way above singly and doubly excited states. According to IPM, there are 50 triply excited states in the $2l2l'3l''$ manifold. These states can decay to singly ionized states of $Li^+ + e$, as well as to doubly ionized states of $Li^{2+} + e + e$. When such decays are not considered, their energies can be obtained approximately using CI approach. The $2l2l'nl''$ triply excited states have been extensively calculated and tabulated using such a method by Conneely and Lipsky [27] for $L \leqslant 3$. We can extract the 49 energy levels of the $2l2l'3l''$ states for $L \leqslant 3$ from their calculation. Their calculated energy levels for Li are shown in Fig. 1, ordered along each column for each $^{2S+1}L^{\pi}$ symmetry. The numerical values are also given in Table I.

From Fig. 1, the level positions appear to be rather erratic. Our objective is to regroup these levels into different subgroups, or to have them classified, such that the energy levels

within each group would exhibit an ordered pattern. The classification is aided by displaying wave functions in appropriate internal coordinates. We analyze the wave functions in hyperspherical coordinates.

The hyperspherical method replaces the radial distances r_1, r_2, and r_3 by a hyper-radius $R=\sqrt{r_1^2+r_2^2+r_3^2}$ and two mock angles $\alpha_1=\tan^{-1}(r_1/r_2)$, $\alpha_2=\tan^{-1}(\sqrt{r_1^2+r_2^2}/r_3)$. The ranges of these variables are $0\leqslant R\leqslant\infty$ and $0\leqslant\alpha_1,\alpha_2\leqslant\pi$. Thus, the nine-dimensional spatial coordinates of the three electrons in the space-fixed frame are represented by the hyper-radius R and eight hyperangles $\{\alpha_1,\alpha_2,\hat{\mathbf{r}}_1,\hat{\mathbf{r}}_2,\hat{\mathbf{r}}_3\}$, where we shall use Ω at times to denote all the eight angles collectively. In hyperspherical coordinates, the Schrödinger equation for the rescaled wave function $\psi=Rr_1r_2r_3\Psi$ is

$$\left[-\frac{1}{2}\frac{\partial^2}{\partial R^2}+H_{\rm ad}(\Omega;R)-E\right]\psi=0, \tag{2}$$

where $H_{\rm ad}(\Omega;R)$ is the adiabatic Hamiltonian which is parametrically dependent on R [44]. Within the adiabatic approximation [45], the total wave function for the nth state in channel μ can be written as

$$\psi_{\mu n}=F_\mu^n(R)\left(\sum_{S_{12}}\Phi_\mu^{S,S_{12}}(\Omega;R)\chi_{S_{12}}^S\right), \tag{3}$$

where $F_\mu^n(R)$ is the hyper-radial function which measures the size of the system; $\Phi_\mu(\Omega;R)$ is the hyperspherical adiabatic channel function, which contains all the information about electron correlations for states within channel μ, and $\chi_{S_{12}}^S=[\{\chi(1)\chi(2)\}^{S_{12}}\chi(3)]^S$ is the total spin function with intermediate spin S_{12}. The channel functions $\Phi_\mu(\Omega;R)$ and their associated adiabatic potentials $U_\mu(R)$ are obtained by solving the adiabatic eigenvalue problem at each R,

$$[H_{\rm ad}(\Omega;R)-U_\mu(R)]\Phi_\mu(\Omega;R)=0. \tag{4}$$

We solve this eight-dimensional eigenvalue problem using basis functions consisting of coupled spherical harmonics for each electron, i.e., products of spherical harmonics in $(\hat{\mathbf{r}}_1,\hat{\mathbf{r}}_2,\hat{\mathbf{r}}_3)$ and direct products of discrete variable representation functions in (α_1,α_2) [44]. In a typical calculation, the orbital angular momentum for each electron ranges from 0 to 3.

As an example, in the top frame of Fig. 2, we show the adiabatic potential curves $U_\mu(R)$ for Li($^2P^o$). The potentials can be classified by their asymptotic limits. At large R, each curve approaches one of the two-electron $\mathrm{Li}^+(nln'l')$ states and it supports the three-electron Li($nln'l'n''l''$) states [46]. In the curves of Fig. 2, there are numerous sharp avoided crossings between the potentials which support the $2l2l'nl''$ triply excited states and those which support the $1snln'l'$ doubly excited states. For clarity, the nine potential curves that support $2l2l'nl''$ triply excited states are shown at the bottom of Fig. 2. These curves are obtained as follows. First, the sharply avoided crossings between the curves that support doubly excited states and those support triply excited states are treated diabatically, i.e., their curves are allowed to cross. Then all the potential curves for singly and doubly excited states are removed. Among the remaining curves that support $2l2l'nl''$ triply excited states, the curves which show sharp avoided crossings are also treated diabatically. Using the diabatic potential curves, each channel function would evolve smoothly such that examination of the channel function for only one particular value of R is adequate to represent the main features of the channel.

Within the single-channel approximation, we can identify the Rydberg series, each curve supports from the asymptotic energy and the position of the minimum of each curve. The nine curves at the bottom frame of Fig. 2 support the nine Rydberg series:

$$\begin{gathered}2s^2(^1S^e)np\\ 2s2p(^3P^o)ns\\ 2s2p(^3P^o)nd\\ 2p^2(^3P^e)np\\ 2p^2(^1D^e)np\\ 2p^2(^1D^e)nf\\ 2s2p(^1P^o)ns\\ 2s2p(^1P^o)nd\\ 2p^2(^1S^e)np\end{gathered} \tag{5}$$

In the Rydberg series in Eq. (5), there are eight states which can be assigned to $2l2l'3l''^2P^o$ triply excited states, since the lowest state in the $2p^2(^1D^e)nf$ series is for $n=4$. The curve which supports the $2p^2(^1D^e)4f$ state can be easily identified from Fig. 2 since it has the potential minimum at the largest values of R among the nine curves at $R\sim10$ a.u. and this curve converges to the $2p^2(^1D^e)$ state of Li^+ at large R. [See Table I for the energy levels of the $\mathrm{Li}^+(2l2l')$ states]. The potential curves that support the two intrashell $2l2l'2l''^2P^o$ states, namely, $2s^22p$ and $2p^3$, can also be easily identified from Fig. 2. Since intrashell states are located at smaller R, each of these two states are supported by the two curves which have the minimum at $R\sim3.5$ a.u.. The $2s^22p$ state is associated with the lowest curve converging to the $2s2p(^3P^o)$ states of Li^+, and the $2p^3$ is associated with the second lowest curve converging to the $2p^2(^3P^e)$ state of Li^+. Thus among the eight $2l2l'3l''^2P^o$ states, two of them are the first excited states of each of these two curves. The other six curves are also identified from their asymptotic behavior and the positions of the potential minima. For each of these six curves, the potential minimum is at $R\sim6$ a.u., and the lowest state is one of the $2l2l'3l''$ states.

B. Analysis and visualization of radial correlations

As discussed in the preceding section, there are nine potential curves that support nine Rydberg series of the $2l2l'nl''^2P^o$ triply excited states. The two curves where the

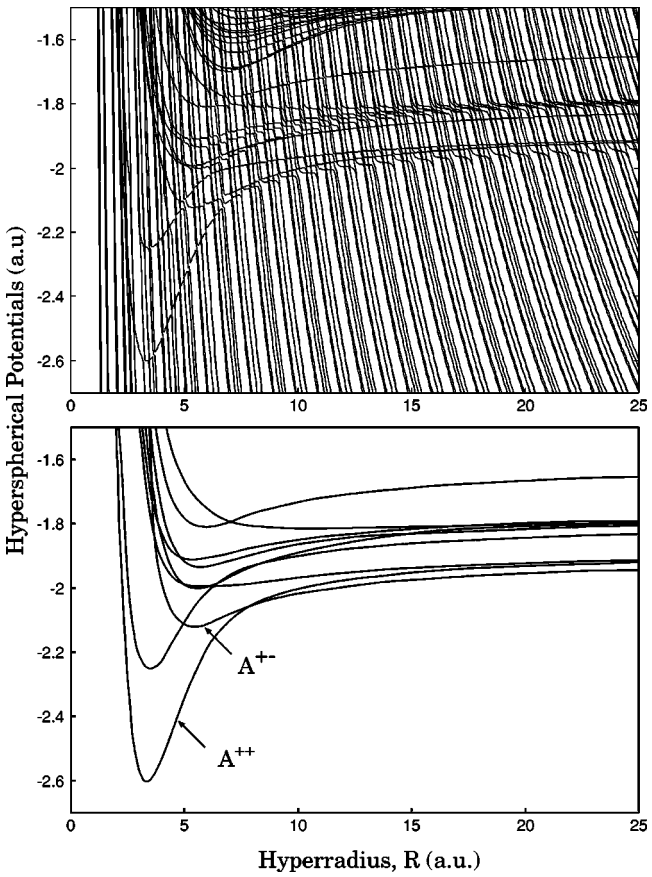

FIG. 2. Hyperspherical potential curves for Li($^2P^o$) in the region of the $2l2l'nl''$ manifolds. Top frame: Adiabatic potentials $U_\mu(R)$. Bottom frame: The nine potential curves which support the $2l2l'nl''$ triply states with the coupling to the potentials for the doubly excited states removed. The potential curve indicated by "A^{++}" supports the $2s^22p^2P^o$ intrashell triply excited state. The potential curve indicated by "A^{+-}" supports the $2s2p(^3P^o)3s^2P^o$ intershell triply excited state.

potential minimum occurs at $R\sim3.5$ a.u. can each support an intrashell $2l2l'2l''$ triply excited state. The rest of the seven curves do not support any intrashell states. The fact that the lowest states have different principal quantum numbers reflects the effect of radial correlations. We can distinguish channels which support intrashell states from those which do not by examining the radial density distribution function at a given R by defining

$$\rho^{\mu}_{\rm rad}(\alpha_1,\alpha_2;R)=\sum_{S_{12}}\int|\Phi^{S,S_{12}}_{\mu}(\Omega;R)|^2 d\hat{\mathbf{r}}_1 d\hat{\mathbf{r}}_2 d\hat{\mathbf{r}}_3. \quad (6)$$

In Fig. 3, we show the results of the densities in the (α_1,α_2) plane for the two channels labeled "A^{++}" and "A^{+-}" in Fig. 2 near their potential minima. In Fig. 3, we divide the (α_1,α_2) plane into six domains separated by dotted lines. Due to the fact that electrons are indistinguishable, the six domains are equivalent. The dotted lines mark the space where two electrons are at the same distance from the nucleus. The point where the three dotted lines intersect is for $r_1=r_2=r_3$. From Fig. 3, it is clear that the radial density

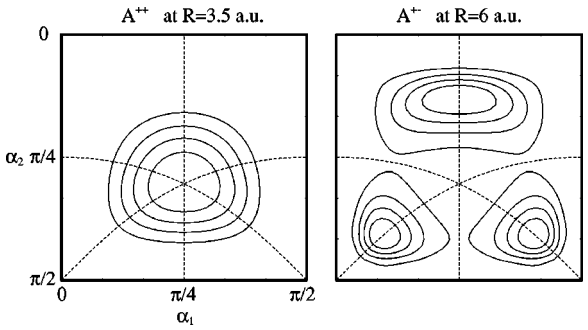

FIG. 3. Illustration of radial electron densities for states in groups A^{++} and A^{+-} in the $^2P^o$ symmetry. Contour plots of the radial density function $\rho^{\mu}_{\rm rad}(\alpha_1,\alpha_2;R)$ at the value of R where the hyperspherical potentials are at the minima, see Fig. 2. The three electrons are at about the same distance from the nucleus for states in group A^{++}, while one of the electrons is at a larger distance from the nucleus than the other two for states in group A^{+-}.

associated with the A^{++} curve has peak at $r_1=r_2=r_3=2.0$ a.u. ($R=3.5$ a.u.), showing the existence of an intrashell $2l2l'2l''$ triply excited state. In contrast, for the A^{+-} curve near the potential minimum at $R=6$ a.u., there is little density at $r_1=r_2=r_3$. Instead, the peak occurs at a point along the dotted line, corresponding to $r_1=r_2=1.6$ a.u. and $r_3=5.5$ a.u., for one of the equivalent peaks, indicating that one electron is further away from the other two as measured from the nucleus.

As will be shown in Secs. III A and III B, the angular part of the channel functions associated with these two curves are almost identical, and they are designated by a symbol "A." Their major difference is in the radial distributions. In the earlier studies of intrashell states, there was no need to address the radial modes of the electrons which are represented by the nodal structure of the distributions in (α_1,α_2). To extend the classification scheme for including $2l2l'3l''$ intershell states, the symmetric or antisymmetric nature of the radial stretch should be described. Pairs of superscripts "$++$" and "$+-$" are used for such purposes. The first superscript for each pair is to describe the phase of the stretch mode of the two inner electrons, while the second one is to describe the phase of the stretch mode of the outermost electron with respect to the two inner ones. For the $++$ states, the radial stretch of all the three electrons are in phase, and their radial motion is totally symmetric. For the $2l2l'3l''$ states treated here, the two inner electrons form a $2l2l'$ intrashell doubly excited state core. Their radial motion is a symmetric stretch mode and thus the first superscript is always "$+$" for the $2l2l'3l''$ states. Note that if we are to classify $2l3l'nl''$ triply excited states, we would encounter "$-$" for the first superscript if the radial stretch for the two inner electrons is antisymmetric, or even "0" if they are "uncorrelated" [6]. In other words, the first superscript is identified with the A quantum number used in the $(K,T)^A$ classification of doubly excited states [6].

The above example shows that we can separate $2l2l'3l''$ states into two groups, namely, $++$ and $+-$, from the radial correlation in the channel functions. However, radial correlation alone does not distinguish the channels within

each group. For example, it does not distinguish the two $++$ channels, nor does it distinguish the seven $+-$ channels. From our previous studies on intrashell states [39,40], each channel within the first group is further distinguished by their angular correlations. For this purpose, we need to analyze the wave functions in the body-fixed frame of the atom.

C. Body-fixed frame analysis of the channel wave functions

The channel function in the laboratory-fixed frame $\Phi^{S,S_{12}}_{\mu\pi LM}$ can be written in terms of the channel function $\varphi^{S,S_{12}}_{\mu\pi LQ}$ in the body-fixed frame by the following transformation:

$$\Phi^{S,S_{12}}_{\mu\pi LM}(\Omega;R)=\sum_{Q=-L}^{L}\varphi^{S,S_{12}}_{\mu\pi LQ}(\Omega_I;R)D^{(L)}_{QM}(\omega), \qquad (7)$$

where $D^{(L)}_{QM}(\omega)$ is the standard rotation matrix, and M and Q are the projections of L onto the space-fixed z axis and the body-fixed $\hat{\mathbf{S}}_z$ axis, respectively. Here, we use ω for the three Euler angles to represent the orientation of the body-fixed frame with respect to the space-fixed system, and the notation Ω_I for the five internal angles to describe the shape of the three-electron atom.

In Eq. (7), the channel function of each Q component $\varphi^{S,S_{12}}_{\mu\pi LQ}$ depends on the choice of the body-fixed frame axes. Following Ref. [11], we define our body-fixed frame by

$$\mathbf{S}_z=\mathbf{r}_1\times\mathbf{r}_2+\mathbf{r}_2\times\mathbf{r}_3+\mathbf{r}_3\times\mathbf{r}_1,$$

$$\mathbf{S}_y=\frac{\sqrt{3}}{2}(\mathbf{r}_1-\mathbf{r}_2),$$

$$\mathbf{S}_x=\mathbf{S}_y\times\mathbf{S}_z. \qquad (8)$$

The body-fixed frame-z axis thus defined is totally antisymmetric and perpendicular to the plane formed by the three electrons. Namely, we consider a three-electron atom as an oblate molecule. In the body-fixed frame, the channel functions satisfy the following relation [11]:

$$\varphi^{S,S_{12}}_{\mu\pi L-Q}(\Omega_I;R)=\pi(-1)^{L+Q}\varphi^{S,S_{12}*}_{\mu\pi LQ}(\Omega_I;R), \qquad (9)$$

where $\pi=\pm1$ is the parity of the system. Thus, we take $T=|Q|$ $(0\leqslant T\leqslant L)$ for analysis in what follows.

In our previous studies of intrashell triply excited states [39,40], the angular correlations of the three electrons were analyzed at $r_1=r_2=r_3$. This particular configuration is equivalent to the model atom where the three electrons are confined to the surface of a sphere. In this case, we defined three angles (θ,η,ϕ) to determine the relative positions of the three electrons on the sphere. For intershell states, in general, the distance of each electron from the nucleus is different. We extend the definition of these angles (θ,η,ϕ) to intershell states. We consider the domain of $(r_3\geqslant r_2\geqslant r_1)$ in what follows. We first define a σ plane formed by the three electrons. Then we define θ to be the angle between the $\mathbf{S}_z$ axis and $\mathbf{r}_1$. It takes two other angles η and ϕ to describe the shape of the triangle of the three electrons. On the σ plane, the angle between electrons 1 and 2 is defined to be 2η, chosen along the arc that includes electron 3. The angle between electron 3 and the line bisecting electrons 1 and 2 is defined to be ϕ. See Fig. 4(a). The ranges of angles are $0\leqslant\theta\leqslant\pi$, $0\leqslant\eta\leqslant\pi$, and $-\eta\leqslant\phi\leqslant\eta$. These three angles, together with α_1, α_2, and R, specify a definite shape and size of the three electrons measured from the nucleus.

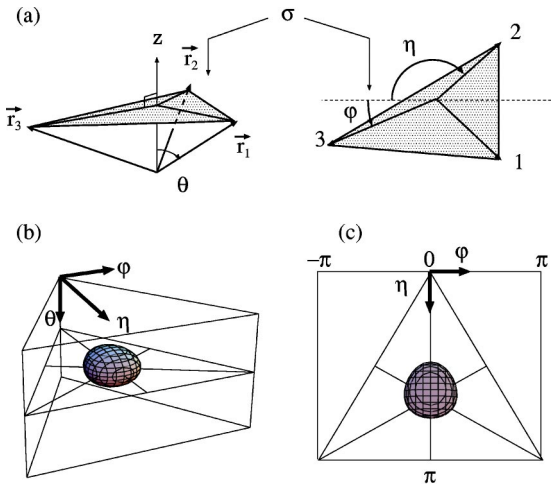

FIG. 4. Definition of the three relative angles among the three electrons and the nucleus for intershell states. (a) The position vectors of the three electrons $(\mathbf{r}_1,\mathbf{r}_2,\mathbf{r}_3)$ from the nucleus form a σ plane. θ is the angle between the z axis of the body-fixed frame and the position vector $\mathbf{r}_1$. The position of the σ plane with respect to the nucleus is measured by θ. On the plane, two angles (η,ϕ) as defined in the figure specify the shape of the triangle formed by the position vectors of the three electrons. (b) Probability distribution of the three electrons on the three angles (θ,η,ϕ) is represented by contour surfaces. (c) Top view of the contour surface to indicate the range of the two angles η and ϕ.

To visualize the collective motion of the three electrons, we introduce the three-electron density function $\rho^{\mu}_{LS\pi T}(\Omega_I;R)$ that is defined as the rotation-averaged density distribution for each channel function,

$$\rho^{\mu}_{LS\pi T}(\Omega_I;R)=\begin{cases}\displaystyle\sum_{S_{12}}|\varphi^{S,S_{12}}_{\mu\pi LT}(\Omega_I;R)|^2 & (T=0)\\ \displaystyle\sum_{S_{12}}[|\varphi^{S,S_{12}}_{\mu\pi L-T}(\Omega_I;R)|^2+|\varphi^{S,S_{12}}_{\mu\pi LT}(\Omega_I;R)|^2] & (T\neq0).\end{cases} \qquad (10)$$

This density represents the probability for the three electrons to take specific shapes. In Fig. 4, we show the density for an intershell state of Li as an example. The plots in Figs. 4(b) and 4(c) represent the contour surfaces where the density is 60% of the maximum at a given (α_1,α_2), taken to be where $\rho^{\mu}_{\rm rad}(\alpha_1,\alpha_2;R)$ [see Eq. (6)] is maximum for the state. A contour surface of higher density would fit inside the surface. Such contour surfaces would provide information on the most probable shape of the three electrons for each triply excited state.

Let us consider the symmetry property of the wave function in the body-fixed frame. Quantum symmetries impose boundary conditions on each rotational component wave function, and play an essential role in the classification. For $2l2l'nl''$ intershell states, two of the electrons in the $n=2$ shell are at the same distance from the nucleus on an average and the third one is further away from the nucleus, i.e., they have maxima at $(r_3>r_2=r_1)$. Here, we consider two important symmetry properties of each T component of intershell $2l2l'nl''$ states at $(r_3>r_2=r_1)$.

First, we study the symmetry due to exchange of the two inner electrons. When $\phi=0$, the three electrons on the σ plane making an isosceles triangle with electrons 1 and 2 at its base. For this geometry, interchange of $\mathbf{r}_1$ and $\mathbf{r}_2$ is equivalent to a rotation of π about the $\mathbf{S}_y$ axis followed by space inversion, $\mathbf{r}\rightarrow-\mathbf{r}$. Under this operation, the internal channel function transforms as $\varphi_{\mu\pi LQ}\rightarrow\pi(-1)^{L+Q}\varphi_{\mu\pi L-Q}$. The interchange of the two electrons 1 and 2 also changes the phase of the channel function due to the antisymmetry, so that $\pi(-1)^{L+Q}\varphi_{\mu\pi L-Q}=(-1)^{S_{12}}\varphi_{\mu\pi LQ}$ for $\phi=0$. This leads to the condition that the internal wave function vanishes at $\phi=0$, when

$$\pi(-1)^{L+S_{12}}=-1 \quad \text{and} \quad T=0. \tag{11}$$

Next, we consider the reflection symmetry with respect to the $(\mathbf{S}_x,\mathbf{S}_y)$ plane in the body-fixed frame. In the coplanar geometry, where the plane of the three electrons contains the nucleus, space inversion is equivalent to a rotation of π about the $\mathbf{S}_z$ axis. Thus under inversion, the internal wave function transforms as $\varphi_{\mu\pi LQ}\rightarrow\pi(-1)^{Q}\varphi_{\mu\pi LQ}$. Thus, the wave function vanishes at $\theta=\pi/2$ for

$$\pi(-1)^{T}=-1. \tag{12}$$

This condition is the same as for intrashell triply excited states [11].

There is no *a priori* reason to expect that each triply excited state possesses only a single major rotational component T in the body-fixed frame. On the other hand, for a highly correlated system if the constituent particles move together similar to that of a rigid body, T would be a good quantum number. By integrating the rotational component density in Eq. (10) over all the angles Ω_I, we obtain a measure of the purity of the rotational component [40],

$$N_T(R)=\frac{1}{8\pi^2}\int \rho^{\mu}_{LS\pi T}(\Omega_I;R)d\Omega_I, \tag{13}$$

where

$$\sum_{T=0}^{L} N_T(R)=1 \tag{14}$$

at each R. If the resulting coefficient $N_T(R)$ is very close to unity, then T is an approximate good quantum number. When this is the case, (θ,η,ϕ) and (α_1,α_2) are considered to be the angles that describe the bending and the stretch modes of an XY_3 molecule, respectively. Thus, to classify triply excited states, one first needs to elucidate to what extent T is a good quantum number, and for that dominant T component where and what is the nature of its nodal surfaces.

In the following, we analyze the channel functions in the body-fixed frame for all $2l2l'3l''$ triply excited states calculated to examine to what extent these states can be classified according to this scheme.

III. CLASSIFICATION OF $2L2L'3L''$ TRIPLY EXCITED STATES

We have calculated the potential curves for Li atom, for all spin and parities, and for $L=0$, 1, 2, 3, and 4. For each symmetry, the curves that support $2l2l'3l''$ triply excited states are identified. These curves are similar to the nine $^2P^0$ curves shown in Fig. 2. We now address the classification of triply excited states by analyzing the channel functions calculated.

A. States belonging to groups A^{++}, B^{++}, and C^{++}

We first identify hyperspherical channels associated with potential curves that support intrashell triply excited states. They are distinguished by having the minimum of the potential at $R\sim3.5$ a.u., as discussed in Sec. II A. For each of such potentials, the $2l2l'3l''$ state is the second state since the first state is a $2l2l'2l''$ intrashell state. For each of such intershell states, the hyper-radial wave function $F_\mu(R)$ has one node, while the channel function is the same as the corresponding intrashell state in the channel. The correlations of the $2l2l'2l''$ intrashell states have been investigated previously. There are eight of them, and are designated as groups I, II, and III earlier [39], but has since been changed to *A*, *B*, and *C* in order to better accommodate the new groups in the classification of $3l3l'3l''$ intrashell triply excited states [37,41]. The states in group *A* are characterized by having the shape of an equilateral triangle with the three electrons at the corners and the nucleus at the center. For states in group *B*, the three electrons have the shape of an equilateral triangle, but the coplanar geometry with the nucleus is forbidden. For states in group *C*, the electrons can be coplanar with the nucleus, but they cannot form an equilateral triangle. We extend this classification to the $2l2l'3l''$ states by adding the radial quantum numbers as superscripts to describe the radial correlation discussed in Sec. II B. Namely, the eight $2l2l'3l''$ states which have the $2l2l'2l''$ intrashell counterparts (i.e., within the same Rydberg series) are assigned to groups A^{++}, B^{++}, and C^{++}.

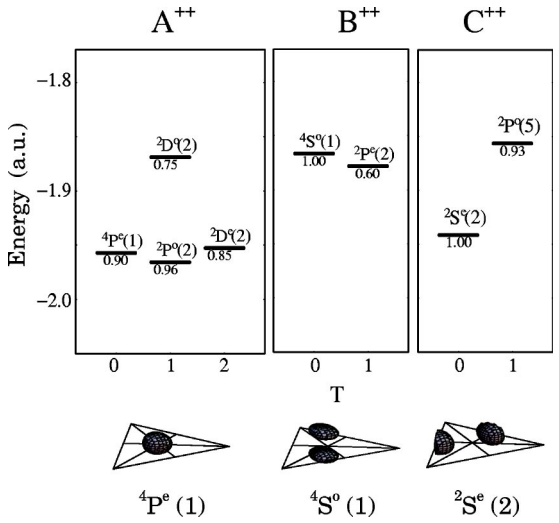

FIG. 5. Energy levels and examples of the three-electron density functions $\rho^{\mu}_{LS\pi T}(\Omega_I;R)$ of the $2l2l'3l''$ triply excited states in groups A^{++}, B^{++}, and C^{++}. Each energy level is denoted by $^{2S+1}L^{\pi}(n)$, where n stands for the nth state within the $2l2l'3l''$ manifold for the given $^{2S+1}L^{\pi}$ symmetry. The hyperangular part of the internal wave functions of the states in groups A^{++}, B^{++}, and C^{++} are the same as those in groups I, II, and III in Ref. [39], respectively.

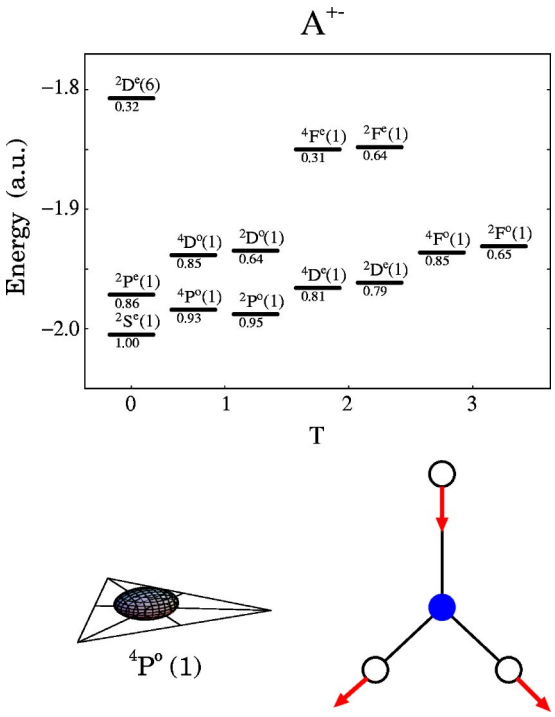

FIG. 6. Energy levels and an example of the density functions of the states in group A^{+-}. Mechanical analog of the motion of the three electrons is shown in the bottom, where the solid circle represents the nucleus and the open circles represent the electrons.

In Fig. 5, we show the energy levels of the eight $2l2l'3l''$ states assigned to A^{++}, B^{++}, and C^{++} groups. In the top frame, the energy levels are ordered according to L and the dominant T component of the state. The integer n in each parenthesis indicates the nth state for that $^{2S+1}L^{\pi}$ symmetry within the $2l2l'3l''$ manifold (Recall, for example, there are eight such $2l2l'3l''^2P^o$ states). The number below each level indicates the rotational purity $N_T(R)$ in Eq. (13) of the state. The closer the purity is to 1, the better the designation is. At the bottom, the rotational density distributions of the dominant T components for representative states are shown. The rotational density distributions for all the states within each group are essentially identical. This is the essence of the classification scheme, indicating that the electronic density distributions in the body-fixed frame for all the states within the group are similar, and the energy levels within the group can be viewed as due to rotational excitations.

We note that the patterns of the energy levels of groups A^{++}, B^{++}, and C^{++} for the $2l2l'3l''$ intershell states are almost the same as those for groups A, B, and C for the intrashell $2l2l'2l''$ states, respectively, since they have the same correlation patterns. We also note that the densities in Fig. 5 are shown at $R\sim 6$ a.u., where the hyper-radial functions of the $2l2l'3l''$ states have the maxima, far away from the locations of the potential minima at $R\sim 3.5$ a.u.. Thus, even though the nodal surfaces remain identical for intershell and the intrashell states, the density distributions are somewhat shifted. For example, the angle between the two inner electrons for the intershell states in groups A^{++} and B^{++} becomes closer to $\pi/2$, since the repulsive force from the outermost electron is weaker than that for intrashell states, and the densities for states in group C have nodal surfaces at $\phi=0$ only.

B. Group A^{+-}

We next identify $2l2l'3l''$ states that have a nodal surface in (α_1,α_2). Clearly, the first group can be designated as group A^{+-}. These states are characterized by an antisymmetric stretch mode of the outer electron with respect to the two inner electrons, as represented by $-$ in the second superscript. This group of states should have no nodal surfaces in the angles (θ,η,ϕ), and thus are designated by symbol A. Not every lowest state of each $+-$ channel belongs to group A^{+-}. From the discussion of the body-fixed frame wave function, certain states exhibit nodal surfaces due to the quantum symmetry. For example, from Eq. (12), if $\pi(-1)^T=-1$, then the body-fixed frame wave function for that T component has a node at $\theta=\pi/2$. Thus only those T components that satisfy $\pi=(-1)^T$ can be assigned to group A^{+-}. In particular, $^2S^o$ and $^4S^o$ states have odd parity and have $T=0$ component only. Consequently, no $^2S^o$ and $^4S^o$ states belong to group A^{+-}. Following the symmetry consideration in Eqs. (11) and (12), and the composition of the rotational components, we have identified the 13 A^{+-} states in Fig. 6. There is one $^2G^e$ state which should be included in this group. This state can be constructed from a $2p^2\ ^1D^e$ core with a $3d$ electron, but it was not calculated by Conneely and Lipsky [27]. From the symmetry consideration and the fraction of the rotational components for the state in Table I, this state should be classified with $T=3$. As a result, there are 14 states in the $2l2'3l''$ manifold that belong to the A^{+-} group. Note that the rotational purity of the low-lying states in the group tends to be much higher. The purity dete-

riorates with increasing L. A low purity is also seen for $^2D^e(6)$ with $T=0$, which is the second $^2D^e$ state in this group.

The 14 states listed in group A^{+-} all have angular distributions characterized by symbol A. The contour surface for a representative state in this group in angles (θ,η,ϕ) is represented in the lower left of Fig. 6. The surface shows that the three electrons tend to lie coplanar with the nucleus, with the three electrons forming an isosceles triangle with the two inner electrons at the base. On the $\theta=\pi/2$ plane, the distribution in (η,ϕ) is rather localized, as seen by the density plot shown in the triangle. The antisymmetric stretch of the outer electron with respect to the two inner symmetric stretch electrons is shown pictorially in Fig. 6 also.

Apart from the antisymmetric stretch mode, a few following observations can be drawn from the rotational level diagrams in Fig. 6.

(1) The energy levels have been ordered similar to the rotational levels of a rigid symmetric top. If the atom can be approximated as a rigid rotor, the energy levels would follow the relation

$$E(L,T)=\frac{2L(L+1)-T^2}{2I}, \tag{15}$$

where I is the moment of inertia. According to this equation, for a given T, the energy levels go up with increasing L. The spectra in Fig. 6 do follow this rule. This equation also states that for a fixed L, the energy decreases with increasing T. Again the energy levels from Fig. 6 do follow this rule. The fact that the energy levels of the states in this group do follow the order of a rigid symmetric top approximately supports the validity of the approximate classification proposed here. In other words, this new classification does identify the essential features common to all the $2l2l'3l''$ triply excited states in this group, in terms of the antisymmetric stretch of the outer electron with respect to the two inner ones and that the three electrons are coplanar with the nucleus and form an isosceles triangle. All these properties are represented by the symbol A^{+-}.

(2) Another observation from Fig. 6 is the near degeneracy of the pair of states that have identical L and T. This is similar to the Λ doubling in molecules. Λ doubling has been found in doubly excited states of atoms as well. Those states with identical K, T, A, and L quantum numbers for nonzero T are nearly degenerate [7].

(3) Another comment to be made is the relative energies of the $2l2l'3l''$ states that belong to group A^{++}, as compared to the states belonging to group A^{+-}. For example, the lowest $2l2l'3l''^2P^o$ state belongs to group A^{+-}, while the second state belongs to group A^{++}. Let us compare the number of nodal surfaces of these two states. Both states have no nodes in angles (θ,η,ϕ). The lowest state belongs to A^{+-}, thus it has a nodal surface in (α_1,α_2), with no node in R. The second state belongs to A^{++}, it has no nodes in (α_1,α_2), but has a node in R. Thus by counting the number of nodes in the first two $2l2l'3l''^2P^o$ states, they have identical number of nodes, but in different coordinates. In a very rough description, these states have identical number of excited quanta, but in different degrees of freedom. In this case, one quantum of excitation in R takes more energy than one quantum of excitation in (α_1,α_2). Such relative energy ordering has been found in two-electron atoms as well. For example, it is known that the $1s2s^3S^e$ state in He has lower energy than the $1s2s^1S^e$ state. From the hyperspherical viewpoint, the latter has a node in the hyper-radial coordinate, while the former has a node in the hyperangle imposed by the symmetry of the state. Similar to the present case, the one with a node in the hyper-radial coordinate has higher energy.

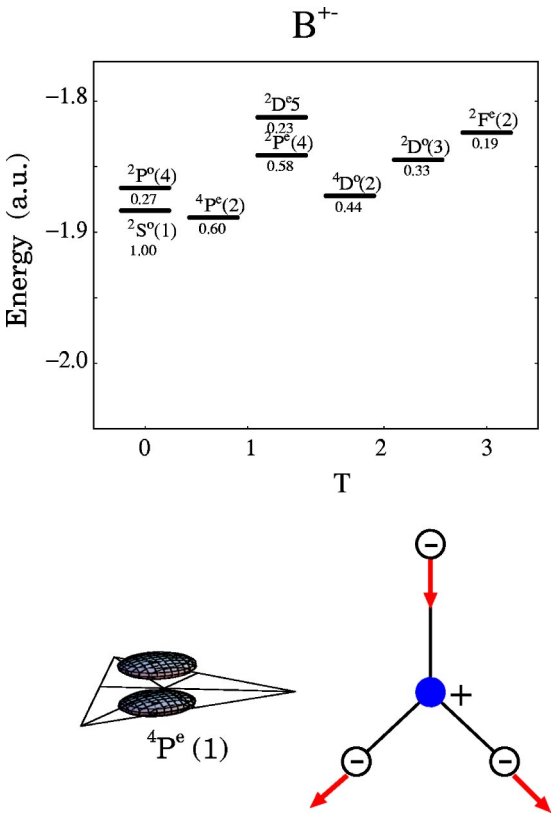

FIG. 7. Same as Fig. 6, but for group B^{+-}.

C. Group B^{+-}

We consider the group of states that have a nodal surface due to the symmetry condition in Eq. (12) at the coplanar geometry, i.e., $\theta=\pi/2$, and where the outer electron has antisymmetric stretch with respect to the two inner ones. We designate this group as B^{+-}, according to our convention. The energy levels of these states are shown in Fig. 7, with a representative distribution in (θ,η,ϕ), shown by the contour surface where the density vanishes at the coplanar geometry. Such a distribution in (θ,η,ϕ) is characteristic of group B. A pictorial representation of the local antisymmetric stretch is shown in the other diagram using arrows, and $+$ and $-$ are used to illustrate the antisymmetric bending vibration with respect to the plane containing the nucleus. Eight states have been identified for this group. This bending vibrational motion is analogous to the bending vibrational motion of NH_3 molecules. Notice that the energies of these states lie be-

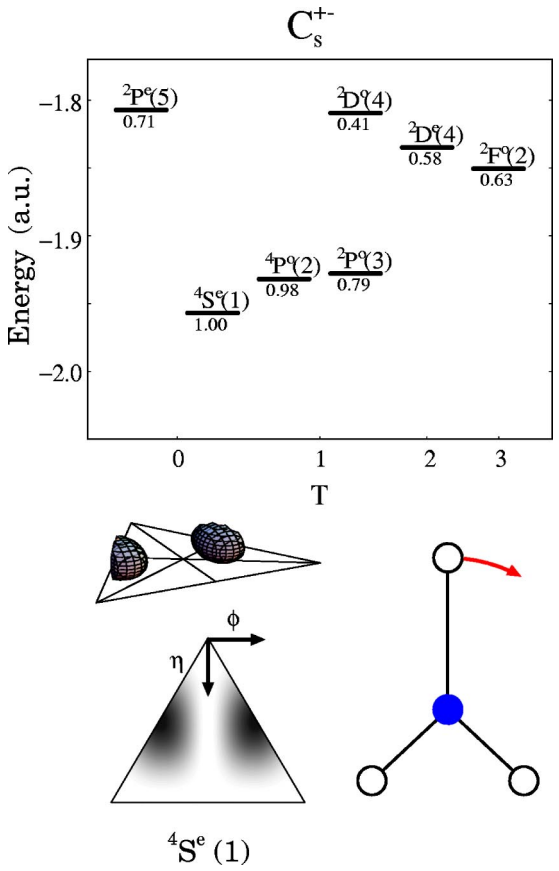

FIG. 8. Energy levels and an example of the density functions of the states in group C_s^{+-}. The density function in (η,ϕ) at $\theta=\pi/2$ is also shown at bottom left. Mechanical analog of the angular motion of the three electrons is shown at the bottom right. The stretch modes in the radial motion are not indicated.

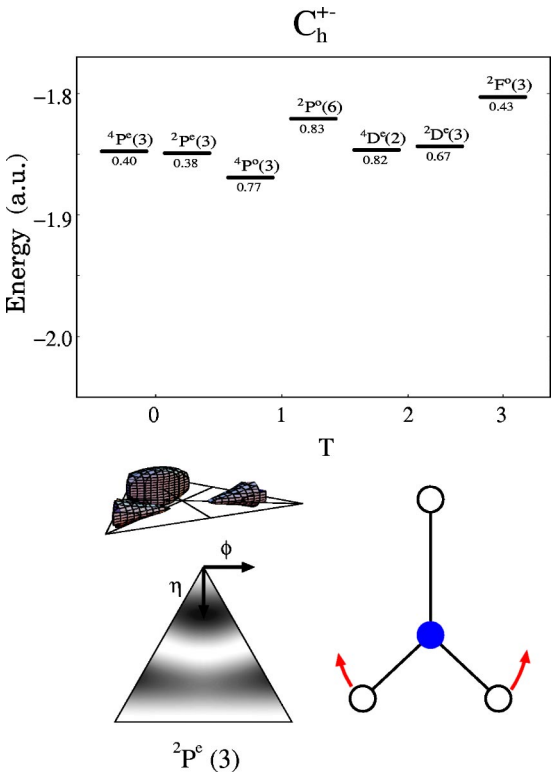

FIG. 9. Same as Fig. 8, but for the C_h^{+-} group.

tween -1.9 and -1.8 a.u.. Referring to Fig. 6, these states have higher energies than most of the states in group A^{+-}. The classification of the higher states within the manifold in terms of collective modes is less accurate since mode mixing is usually not small.

D. Groups C_s^{+-} and C_h^{+-}

The next groups that we identified are labeled as C_s^{+-} and C_h^{+-}. The radial motion of the outermost electron exhibits antisymmetric stretch with respect to the two inner ones. The wave functions tend to distribute near the $\theta=\pi/2$ plane, as seen from the contour surface plots in Figs. 8 and 9. The designations of C_s and C_h are to distinguish the nodal surfaces in ϕ and in η, respectively, and to give each a mechanistic interpretation, as illustrated pictorially in Figs. 8 and 9. (Only angular motions are illustrated in the figures, although they also have the $+-$ type radial stretch motion.)

For group C_s^{+-}, there is a nodal plane at $\phi=0$ and this is understood as a swing motion of the outer electron, with the two inner elections more or less fixed. We note that the nodal surface of the $^4S^e(1)$ state is due to the symmetry condition in Eq. (11), while the nodes of the other states in group C_s^{+-} are due to a dynamic excitation of the angular mode. Similarly, group C_h^{+-} designates states where the two inner electrons perform a hinge motion, with the outer electron more or less fixed. A node in the wave function at $\eta\sim\pi/4$ due to the excitation of the angular mode is the major feature of these states. This node is clearly seen in the (η,ϕ) plane and is illustrated mechanically as well.

We emphasize that both groups C_s^{+-} and C_h^{+-} are characterized by the fact that an isosceles triangle in the plane of the nucleus is unfavorable, or more precisely, for the dominant T component the wave function vanishes at this special geometry. For intrashell states, we cannot distinguish the swing mode from the hinge mode, since they are degenerate. A single mode was used for the intrashell states [39,37,41]. For intershell states, the hinge motion is between the two inner electrons, while the swing motion is for the outer electron. Thus, the degeneracy in these two modes disappears.

E. Groups C_{ss}^{+-}, C_{hh}^{+-}, and C_{sh}^{+-}

The last groups consist of excited states constructed from C_s^{+-} and C_h^{+-} groups. They are assigned to three groups, C_{ss}^{+-}, C_{hh}^{+-}, and C_{sh}^{+-}, as shown in Fig. 10, together with examples of the density functions. These are highly excited states within the $2l2l'3''$ manifold and the number of their members are severely truncated as imposed by the IPM and the Pauli exclusion principle. There is only one state in group C_{ss}^{+-}, namely, $^2S^e(4)$ with $T=0$. The density function of this state in group C_{ss}^{+-} has two nodal surfaces at $\phi=$const. Each state in this group has one more quantum in the swing mode (s) comparing to the states in group C_s^{+-}. Thus, the states are designated by C_{ss}^{+-}, having two s's in

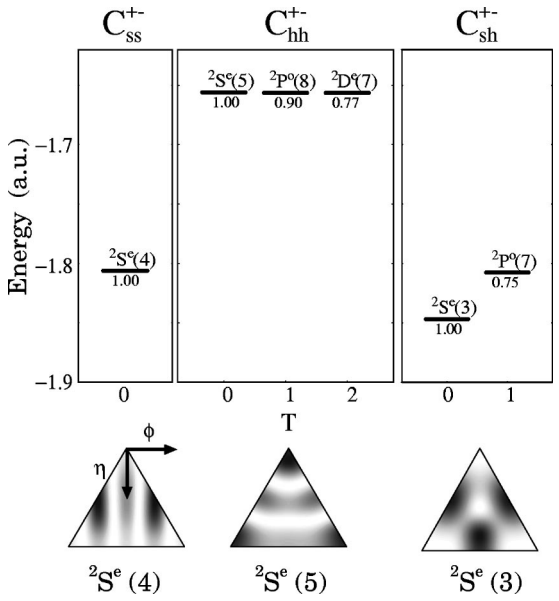

FIG. 10. Energy levels and examples of the density functions of the states in groups C^{+-}_{ss}, C^{+-}_{hh}, and C^{+-}_{sh}. The density functions are in the (η,ϕ) plane at $\theta=\pi/2$.

the subscripts. Similarly, we identified group C^{+-}_{hh} by adding an extra nodal surface in angle η to states in group C^{+-}_{h}. Three states are assigned in this group as shown in Fig. 10. We also have group C^{+-}_{sh} and two states in this group are shown in Fig. 10. These states have additional nodal surfaces in (η,ϕ). For these states, the hinge mode and the swing mode are mixed together, and their nodal surfaces are not parallel either to ϕ axis or to η axis. We tentatively designate them as belonging to group C^{+-}_{sh}. For these higher excited states, the densities are not very localized, so the assignment presented here may be questionable. However, it shows our attempt at classifying these higher states based on the rovibrational model of a molecule.

IV. SUMMARY AND CONCLUSION

In this paper, we proposed a classification scheme for the intershell $2l2l'3l''$ triply excited states of atoms. Compared to intrashell states, the opening of the stretch mode of the outer electron with respect to the two inner ones introduces many more states. We have classified eight of these states into groups A^{++}, B^{++}, and C^{++} which are the extension from the $2l2l'2l''$ intrashell states. The rest of the 42 states have been found to belong to groups A^{+-}, B^{+-}, C^{+-}_{s}, C^{+-}_{h}, C^{+-}_{ss}, C^{+-}_{hh}, and C^{+-}_{sh}. Symbols *A*, *B*, and *C* with subscripts *s* and *h* are used to denote the bending vibrational modes. The pairs of superscripts "++" or "+−" are used to denote the symmetric or antisymmetric stretch modes: The first superscript is for the motion of the two inner electrons, and the second superscript is for the motion of the outer electron with respect to the two inner electrons. The final results from the present classifications are summarized in Table I. Under column 1, each state is labeled by its L, S, π, and n of the nth state within that symmetry in the $2l2l'3l''$ manifold. The second column gives the classification of that state from the present work. Along the third column, the IPM designation by Conneely and Lipsky [27] is shown. The fourth column gives the energy of the state obtained by Conneely and Lipsky [27]. The remaining coefficients give the rotational compositions of the wave function in the body-fixed frame at the hyper-radius R_0 indicated. R_0 was chosen to be near where the hyper-radial wave function is maximum for that state.

The scheme presented here could possibly be generalized to triply excited states where all the three electrons are in different shells, such as $2l3l'4l''$ states. In this case, there will be symmetric and antisymmetric stretches between the two inner electrons, corresponding to + and − for the first superscript, in addition to the + and − for the second superscript addressed here. The classification of these states would be extremely tedious and difficult since the deviation from the simple normal modes in each degree of freedom would be very large. Unlike complex molecules where experimentalist can excite one or two bonds between a pair of atoms, the identification of different modes in multiply excited states is extremely complicated since they are truly many body in nature. Our attempt for the triply excited intrashell and intershell states of atoms in the past years shows the complexities of such an endeavor. With high excitation energies and high density of these states within a narrow energy region, progress both in theory and experiment is expected to be very slow. On the other hand, using the procedure employed in this paper for the classification of $2l2l'3l''$ states, the method can, in principle, be extended to higher triply excited states even though the actual classification would be very complicated.

ACKNOWLEDGMENTS

T.M. wishes to thank Professor M. Matsuzawa and Professor S. Watanabe for their encouragement throughout this work. T.M. was supported in part by a Grant-in-Aid for Scientific Research, Ministry of Education, Science, and Culture, Japan, and C.D.L. was supported in part by Chemical Sciences, Geosciences and Biosciences Division, Office of Basic Energy Sciences, Office of Science, U.S. Department of Energy.

[1] D.R. Herrick and O. Sinanoğlu, Phys. Rev. **11**, 97 (1975).
[2] O. Sinanoğlu and D.R. Herrick, J. Chem. Phys. **62**, 886 (1975).
[3] M.E. Kellman and D.R. Herrick, J. Phys. B **11**, L755 (1978).
[4] M.E. Kellman and D.R. Herrick, Phys. Rev. A **22**, 1536 (1980).
[5] G.S. Ezra and R.S. Berry, Phys. Rev. A **28**, 1974 (1983).
[6] C.D. Lin, Phys. Rev. A **29**, 1019 (1984).
[7] S. Watanabe and C.D. Lin, Phys. Rev. A **34**, 823 (1986).
[8] J.W. Cooper, U. Fano, and F. Prats, Phys. Rev. Lett. **10**, 518 (1963).

[9] G. Tanner *et al.*, Rev. Mod. Phys. **72**, 49 (2000).
[10] C. Yannouleas and U. Landman, Phys. Rev. Lett. **85**, 1726 (2000).
[11] S. Watanabe and C.D. Lin, Phys. Rev. A **36**, 511 (1987).
[12] C.G. Bao, X. Yang, and C.D. Lin, Phys. Rev. A **55**, 4168 (1997).
[13] K. Berrington and S. Nakazaki, J. Phys. B **31**, 313 (1998).
[14] L. VoKy, P. Faucher, H.L. Zhou, A. Hibbert, Y.-Z. Qu, J.M. Li, and F. Bely-Dubau, Phys. Rev. A **58**, 3688 (1998).
[15] H.L. Zhou, S.T. Manson, L. VoKy, P. Faucher, F. Bely-Dubau, A. Hibbert, S. Diehl, D. Cubaynes, J.-M. Bizau, L. Journel, and F.J. Wuilleumier, Phys. Rev. A **59**, 462 (1999).
[16] H.L. Zhou, S.T. Manson, P. Faucher, and L. VoKy, Phys. Rev. A **62**, 012707 (2000).
[17] C.A. Nicolaides, N.A. Piangos, and Y. Komninos, Phys. Rev. A **48**, 3578 (1993).
[18] C.A. Nicolaides and N.A. Piangos, J. Phys. B **34**, 99 (2001).
[19] K.T. Chung and B.C. Gou, Phys. Rev. A **52**, 3669 (1995).
[20] K.T. Chung and B.C. Gou, Phys. Rev. A **53**, 2189 (1996).
[21] Y. Zhang and K.T. Chung, Phys. Rev. A **58**, 3336 (1998).
[22] L.B. Madsen, P. Schlagheck, and P. Lambropoulos, Phys. Rev. A **62**, 062719 (2000).
[23] T.K. Fang and K.T. Chung, Phys. Rev. A **63**, 020702 (2001).
[24] K.T. Chung and T.K. Fang, Phys. Rev. A **63**, 062716 (2001).
[25] G. Verbockhaven and J.E. Hansen, Phys. Rev. Lett. **84**, 2810 (2000).
[26] M.J. Conneely and L. Lipsky, Phys. Rev. A **61**, 032506 (2000).
[27] M. J. Conneely and L. Lipsky, At. Data Nucl. Data Tables **482**, 115 (2002).
[28] L.M. Kiernan, M.-K. Lee, B.F. Sonntag, P. Sladeczek, P. Zimmermann, and E.T. Kennedy, J. Phys. B **28**, L161 (1995).
[29] Y. Azuma, S. Hasegawa, F. Koike, G. Kutluk, T. Nagata, E. Shigemasa, A. Yagishita, and I.A. Sellin, Phys. Rev. Lett. **74**, 3768 (1995).
[30] Y. Azuma, F. Koike, J.W. Cooper, T. Nagata, G. Kutluk, E. Shigemasa, R. Wehlitz, and I.A. Sellin, Phys. Rev. Lett. **79**, 2419 (1997).
[31] L. Journel, D. Cubaynes, J.-M. Bizau, S. Al Moussalami, B. Rouvellou, F.J. Wuilleumier, L. VoKy, P. Faucher, and A. Hibbert, Phys. Rev. Lett. **76**, 30 (1996).
[32] S. Diehl, D. Cubaynes, J.-M. Bizau, L. Journel, B. Rouvellou, S. Al Moussalami, F.J. Wuilleumier, E.T. Kennedy, N. Berrah, C. Blancard, T.J. Morgan, J. Bozek, A.S. Schlachter, L. VoKy, P. Faucher, and A. Hibbert, Phys. Rev. Lett. **76**, 3915 (1996).
[33] S. Diehl, D. Cubaynes, K.T. Chung, F.J. Wuilleumier, E.T. Kennedy, J.-M. Bizau, L. Journel, C. Blancard, L. VoKy, P. Faucher, A. Hibbert, N. Berrah, T.J. Morgan, J. Bozek, and A.S. Schlachter, Phys. Rev. A **56**, R1071 (1997).
[34] S. Diehl, D. Cubaynes, F.J. Wuilleumier, J.-M. Bizau, L. Journel, E.T. Kennedy, C. Blancard, L. VoKy, P. Faucher, A. Hibbert, N. Berrah, T.J. Morgan, J. Bozek, and A.S. Schlachter, Phys. Rev. Lett. **79**, 1241 (1997).
[35] D. Cubaynes, S. Diehl, L. Journel, B. Rouvellou, J.-M. Bizau, S. Al Moussalami, F.J. Wuilleumier, N. Berrah, L. VoKy, P. Faucher, A. Hibbert, C. Blancard, E. Kennedy, T.J. Morgan, J. Bozek, and A.S. Schlachter, Phys. Rev. Lett. **77**, 2194 (1996).
[36] Y. Zhang and K.T. Chung, Phys. Rev. A **58**, 1098 (1998).
[37] T. Morishita and C.D. Lin, J. Phys. B **31**, L209 (1998).
[38] T. Morishita, C.D. Lin, and C.G. Bao, Phys. Rev. Lett. **80**, 464 (1998).
[39] T. Morishita, Y. Li, and C.D. Lin, Phys. Rev. A **58**, 4214 (1998).
[40] T. Morishita and C.D. Lin, Phys. Rev. A **59**, 1835 (1999).
[41] T. Morishita and C.D. Lin, Phys. Rev. A **64**, 052502 (2001).
[42] L.B. Madsen and K. Mølmer, Phys. Rev. Lett. **87**, 133002 (2001).
[43] L.B. Madsen and Mølmer, Phys. Rev. A **65**, 022506 (2002).
[44] T. Morishita and C.D. Lin, Phys. Rev. A **57**, 4268 (1998).
[45] J. Macek, J. Phys. B **1**, 831 (1968).
[46] T. Morishita, O.I. Tolstikhin, S. Watanabe, and M. Matsuzawa, Phys. Rev. A **56**, 3559 (1997).